

# Dramatic robustness of a multiple delay dispersed interferometer to spectrograph errors: how mixing delays reduces or cancels wavelength drift

David J. Erskine<sup>a</sup>, E. Linder<sup>b</sup>, E. Wishnow<sup>c</sup>, J. Edelstein<sup>c</sup>, M. Sirk<sup>c</sup>, P. Muirhead<sup>d</sup>, J. Lloyd<sup>e</sup>,  
A. Kim<sup>b</sup>

<sup>a</sup>Lawrence Livermore Nat. Lab., Livermore, CA 94550

<sup>b</sup>Lawrence Berkeley Nat. Lab., Berkeley, CA 94720

<sup>c</sup>Space Sciences Lab., Univ. of Calif., Berkeley, CA 94720

<sup>d</sup>Astronomy Dept., Boston University, Boston, MA 02215

<sup>e</sup>Carl Sagan Inst., Astron. Dept., Cornell University, Ithaca NY, 14853

## ABSTRACT

We describe demonstrations of remarkable robustness to instrumental noises by using a *multiple delay* externally dispersed interferometer (EDI) on stellar observations at the Hale telescope. Previous observatory EDI demonstrations used a single delay. The EDI (also called “TEDI”) boosted the 2,700 resolution of the native TripleSpec NIR spectrograph (950-2450 nm) by as much as 10x to 27,000, using 7 overlapping delays up to 3 cm. We observed superb rejection of fixed pattern noises due to bad pixels, since the fringing signal responds only to changes in multiple exposures synchronous to the applied delay dithering. Remarkably, we observed a  $\sim 20x$  reduction of reaction in the output spectrum to PSF shifts of the native spectrograph along the dispersion direction, using our standard processing. This allowed high resolution observations under conditions of severe and irregular PSF drift otherwise not possible without the interferometer. Furthermore, we recently discovered an improved method of weighting and mixing data between pairs of delays that can theoretically further reduce the net reaction to PSF drift to zero. We demonstrate a 350x reduction in reaction to a native PSF shift using a simple simulation. This technique could similarly reduce radial velocity noise for future EDI’s that use two delays overlapped in delay space (or a single delay overlapping the native peak). Finally, we show an extremely high dynamic range EDI measurement of our ThAr lamp compared to a literature ThAr spectrum, observing weak features ( $\sim 0.001x$  height of nearest strong line) that occur between the major lines. Because of individuality of each reference lamp, accurate knowledge of its spectrum between the (unfortunately) sparse major lines is important for precision radial velocimetry.

**Keywords:** High resolution spectroscopy, Externally Dispersed Interferometry, Dispersed Fixed Delay Interferometry, Resolution Boosting, Doppler radial velocimetry, Fourier Transform Spectroscopy, Exoplanets

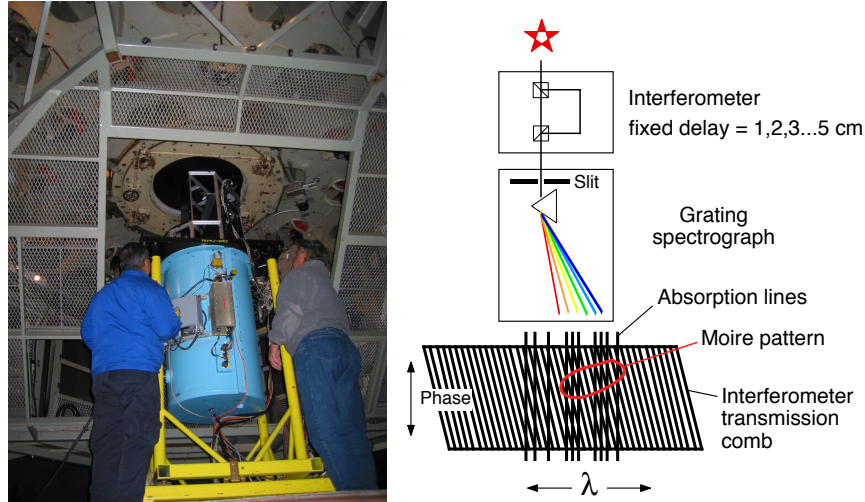


Figure 1. (Left) The T-EDI interferometer (black & silver) sits atop TripleSpec (native) spectrograph (blue cryogenic cylinder) which bolts to Cassegrain output (39 inch diameter cavity) of the Mt. Palomar 200 inch mirror. (Middle) (Right) Externally Dispersed Interferometer (EDI) scheme— a fixed delay interferometer is crossed with a disperser. The sinusoidal transmission of the interferometer creates moire patterns whose phase encodes the Doppler velocity and whose shape encodes the spectrum’s shape. The interferometer measures the details of the spectra, while the disperser separates the wavelengths to enhance fringe visibility.

## 1. OVERVIEW

### 1.1 Externally Dispersed Interferometry

A novel technique called externally dispersed interferometry<sup>1</sup> (EDI) can dramatically reduce the necessary size of spectrographs for Doppler radial velocimetry<sup>1-9</sup> and high resolution spectroscopy,<sup>10-17</sup> and dramatically increase their robustness to PSF errors in the native spectrograph. Other workers have adopted the EDI method from our laboratories and demonstrated a Doppler planet detection.<sup>4</sup> We have demonstrated EDI in both applications in the near-infrared at the Hale 5-m telescope at Mt. Palomar Observatory (Fig. 1) with a version called TEDI, (the T denotes the TripleSpec<sup>18</sup> spectrograph to which it was coupled). An earlier report<sup>7</sup> describes the Doppler velocimetry, and this report describes the spectroscopy.

Figure 2b is an example of EDI resolving a closely spaced ThAr line pair (red curve) otherwise unresolvable by the native spectrograph (green curve). Fig. 2a shows how the EDI output is a sum over multiple wavelets, each wavelet period proportional to the interferometer delay. The envelope of the wavelet is controlled by the native spectrograph, while the phase of the wavelet (which determines the narrow feature position) is controlled by the interferometer. The latter is independent of the native spectrograph and its distortions. Hence, this produces the great robustness of EDI to native PSF distortions.

The interferometer phase is subject to its own drift, which is due to mechanical repositioning changes in the delay as we swap out etalons for different exposures, for each stellar target. This offset is removed by observation of ThAr spectra lamp lines co-measured with the stellar spectra. The sinusoidal nature of the fringes (having only three degrees of freedom) is much easier to calibrate out than the PSF of the grating spectrograph, which has many more degrees of freedom (potentially one per grating groove involved). For example, the sinusoidal comb across the entire band will shift monolithically, maintaining its sinusoidal character, whereas for the native spectrograph the PSF distortion can vary *irregularly* vs wavelength due to the large number of grating grooves involved in forming the PSF shape (seen in our native spectrograph data Fig. 3). This makes it impossible to correct the irregular PSF distortion with a simple adjustment.

This is the first time multiple delays have been used on starlight to recreate high resolution spectra. Previous resolution boosting demonstrations on stellar spectra used a single delay,<sup>11</sup> (multiple delays had been used

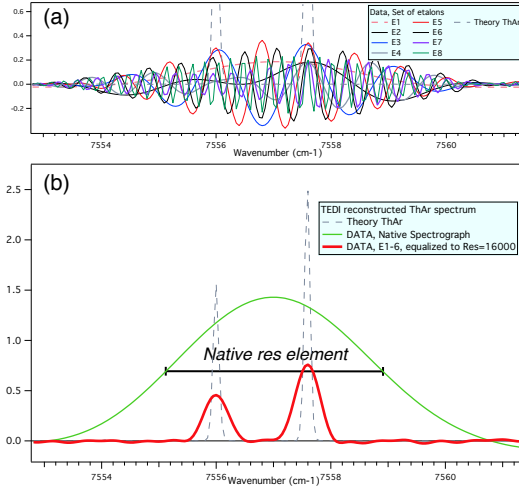


Figure 2. (a) Reconstruction of an otherwise unresolved ThAr doublet ( $7556, 7557.6 \text{ cm}^{-1}$ ) from many wavelets measured at multiple delays. (b) The native spectrograph (green curve) cannot resolve the doublet. The EDI reconstructed spectrum (red curve), which is sum of wavelets, then equalized to  $\text{res}=16000$ , easily resolves the doublet.

previously<sup>12</sup> on laboratory sources). Reference 16 is a comprehensive report on TEDI data analysis procedure, example output spectra, and instrumental noise analysis. A theoretical photon noise analysis is in Ref. 17.

The TEDI project was designed primarily to test Doppler measurements, and the selection of interferometer glass etalons and observing schedule was prioritized for this purpose. These were not optimal for testing high resolution spectroscopy (having a gap in coverage of delay space when contiguous coverage is needed to avoid ringing in the final lineshape). Nevertheless, the demonstration results for high resolution spectroscopy using multiple delays is a resounding success in two important areas.

### 1.2 Resolution, Robustness Demonstrated

We have demonstrated on starlight that EDI technique can produce both high resolution, a factor of 4x to 10x beyond the native spectrograph resolution of  $\sim 2700$ , and have extremely wide simultaneous bandwidth, limited only by the bandwidth of the native spectrograph ( $0.95 - 2.45 \mu\text{m}$ ). Secondly, the native spectrograph in our study suffered from extremely large and irregular PSF drifts that would normally have precluded the high resolution we obtained, even if by some other means the slit width and focal spot had been reduced by several times, and the detector pixel density increased. (The TEDI data set is instrument limited rather than photon limited.) A great advantage of the EDI technique, especially when used with *multiple* delays rather than a single delay as used previously, is an order of magnitude or more improvement in the stability against PSF drifts.

Remarkably, we observed a  $\sim 20\text{x}$  reduction of reaction in the output spectrum to PSF shifts of the native spectrograph along the dispersion direction, using our standard processing. This allowed high resolution observations under conditions of severe and irregular PSF drift otherwise not possible without the interferometer.

Furthermore, we recently discovered an improved method of weighting and mixing data between pairs of delays that can theoretically further reduce the net reaction to PSF drift to zero. We demonstrate a 350x reduction in reaction to a native PSF shift using a simple simulation. This technique could similarly reduce radial velocity noise for future EDI's that use two delays overlapped in delay space (or a single delay overlapping the native peak).

## 2. EXAMPLE OUTPUT SPECTRA

Figure 4(a) shows the useful bandwidth of TEDI extending over four orders, and (d) zooms in to a single telluric feature, demonstrating the remarkably high resolution-bandwidth product. Figure 5 compares two stars measured nearly simultaneously at a 6x resolution boost.

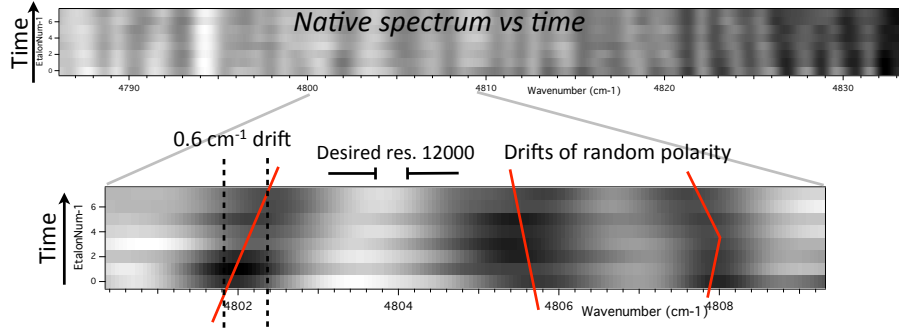


Figure 3. Example of the large PSF irregularity in the native spectrograph. This is a stack of eight native spectra of A-order ( $4000\text{--}5100\text{ cm}^{-1}$ ), one per etalon (EtalonNum), used in the multiple delay EDI. The Y-axis is EtalonNum, which is therefore also vs time,  $\sim 10$  minutes apart, since the eight available etalons E1-E8 were used approximately sequentially. To produce these native spectra, the embedded interferometer fringes have been removed from the raw data by summing over phase steps. (The native spectra component is more useful for illustrating wavelength drift since its features are independent of delay.) The linear PSF shift vs EtalonNum is called “shear”. Bulk shear has already been removed from every row here, and a residual irregularity as high as  $\sim 0.6\text{ cm}^{-1}$  remains. Note the polarity of the shear flips for neighboring wavenumber regions, preventing further bulk removal and making correction by usual math operations impractical.

Figure 6 shows extremely high dynamic range measurement of small ( $\sim 0.1\%$  nearest bright line) features of our ThAr lamp compared to the ThAr lamp of NIST. This shows that while our Ar line heights agree perfectly with NIST, our Th lines are smaller by a factor of several. ThAr lamps are known to be individual in their characteristics, and it is valuable to measure the particular ThAr lamp being used, since minor differences can affect the result for the large portions of the spectra between the major lines.

### 3. FIXED PATTERN NOISE REJECTION

We observed superb rejection of fixed pattern noises due to bad pixels, since the fringing signal responds only to changes in multiple exposures synchronous to the applied delay dithering. These pollute the native spectrum but not the EDI derived spectrum, measured simultaneously. The superb rejection of bad pixels is shown by Fig. 6 (at  $9174\text{ cm}^{-1}$  and  $9214\text{ cm}^{-1}$ ), and Fig. 7 (at  $5015\text{ cm}^{-1}$  and the entire red end of A-order  $<4200\text{ cm}^{-1}$ ).

### 4. LARGE DRIFTS IN NATIVE SPECTROGRAPH DEFEATED BY EDI

Figure 3 shows the extremely large and irregular drifts in our native PSF vs time (actually versus etalon number, but this changes roughly with time every few minutes). The drifts are easier to detect by displaying the native spectrum, rather than the original fringing spectrum, because the native spectrum has features that are not affected by the fringes. Yet note the large  $0.6\text{ cm}^{-1}$  drift across the etalons at  $4802\text{ cm}^{-1}$ . Even more surprising, not that the drift at nearby  $4808\text{ cm}^{-1}$  is in the *opposite* direction vs time. Hence this type of irregularity is not removed by a bulk shift across the band. This amount of irregular PSF drift would normally prevent the type of high resolution seen in the EDI output, even if the resolution were somehow able to be increased by classical means (such as slit narrowing and increase density of pixels).

Figure 8 demonstrates of how the high resolution output, in panel (a) between the dashed and solid red curves, does not depend significantly on the two different cases of the PSF shift (slant vs etalon #), seen between panels (b) and (c).

Figure 9 is a simulation using TEDI data of a ThAr line at  $4849\text{ cm}^{-1}$  that is artificially shifted toward the left by  $0.5\text{ cm}^{-1}$ , for all etalons, using original lineshapes. The before (b) and after (c) stack of wavelets show how the envelope is shifted, and the underlying wavelet phase is mostly unchanged. (The lowest delays having the broadest features which are most similar in width to the native PSF width are the most susceptible to envelope change. The shift in the output peak between the original (thin red) and shifted (thin black dashes)

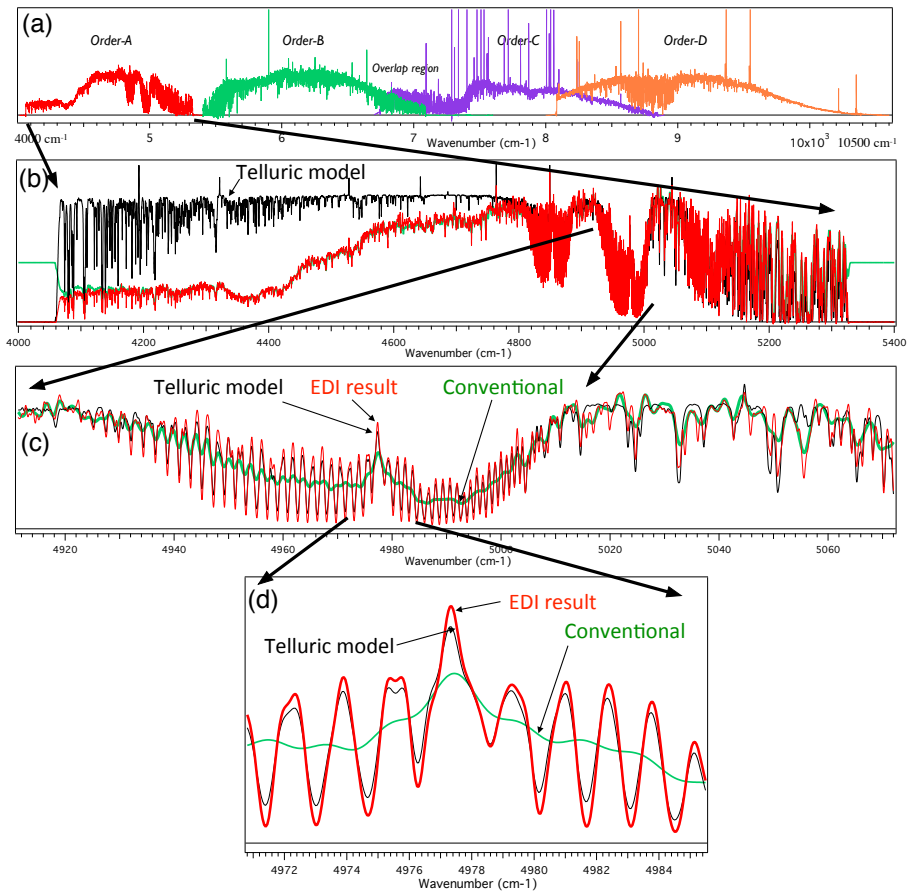


Figure 4. An externally dispersed interferometer preserves the wide bandwidth of the native spectrograph while boosting the resolution, so that the product of bandwidth times resolution increases by a factor of several. In contrast, in a conventional spectrograph the bandwidth resolution product is usually constant, limited by number of detector pixels. (a) This TEDI reconstructed spectrum spans 4 orders of the TripleSpec echelle spectrograph in the NIR ( $4100\text{-}10500\text{ cm}^{-1}$ ), observing HD219134 at resolution 11000 (4x boost). Panels (b, c, d) zoom in telluric feature near  $\sim 4980\text{ cm}^{-1}$  due to  $\text{CO}_2$  molecule.

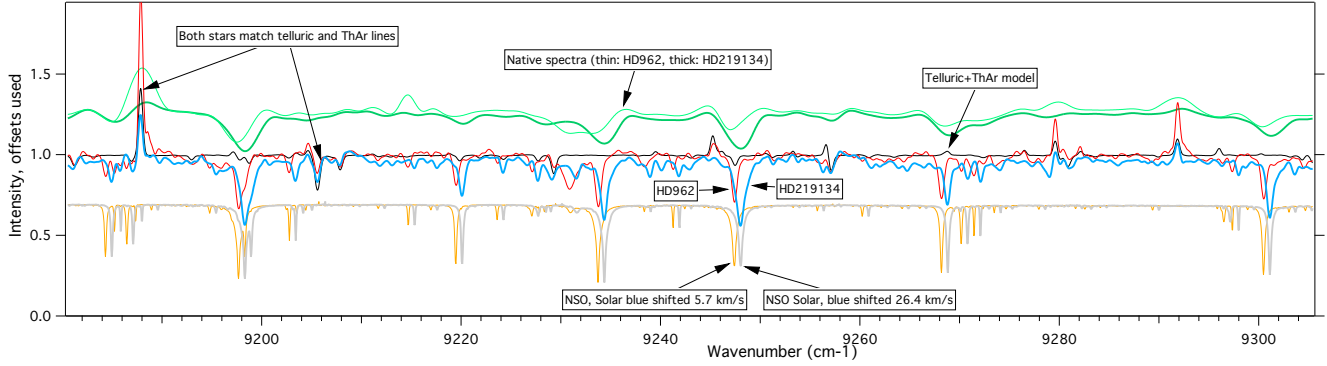


Figure 5. Comparing two stars measured nearly simultaneously, HD962 (red curve), and HD219134 (blue curve) on 2015 Sep 19 around UT of 10 hours, in the D-order ( $\sim 9200 \text{ cm}^{-1}$ ). Resolution is 19000, a 6x boost over native spectra (thin and thick green curves for HD962 and HD219134). The SIMBAD database classifies HD962 as a featureless A-type star. However we find stellar absorption lines of similar depth as to HD219134, which is K-type. Secondly, we measure for HD962 a Doppler velocity that differs significantly from its SIMBAD value, (29 km/s too red– the HD962 lines should be bluer than HD219134, not redder), whereas for HD219134 it agrees perfectly. The ThAr and telluric features of HD962 agree nicely with theory (see 9188 and 9206  $\text{cm}^{-1}$ ), the same difference in Doppler velocity observed here in the D-order is observed in the A-order (4100-5300  $\text{cm}^{-1}$ ), and consistent with the shift seen between low res native spectra (thin to thick green curves), so we believe the measurement is accurate.

peaks is only  $0.025 \text{ cm}^{-1}$ . This is 20 times smaller than the applied shift of  $0.5 \text{ cm}^{-1}$ . Hence the robustness to PSF shift error is about a factor of 20x, for the standard EDI processing done here (not using the strategic crossfading weighting or reshaping technique introduced below).

This factor of 20x of robustness is remarkable, and is due to the use of multiple delays and the basic interferometer nature of EDI relative to the native spectrograph, as depicted notionally in Fourier space in Fig. 10. The reaction to a displacement of the PSF in wavenumber or pixel space creates a twist (slope in phase vs  $\rho$ ) of the Fourier expression of the signal. This slope increases linearly with frequency ( $\rho$ ). Hence we have drawn red lines in Fig. 10 which pass through zero at the center of each  $psf(\rho)$  peak, and native peak.

#### 4.1 Conventional Case

For the conventional case (Fig. 10(a)), note that the native spectrograph peak and red line is centered at zero frequency. Thus its reaction increases linearly with  $\rho$ , and by the time it gets to the higher frequencies where science signals typically reside, it is a large error effect.

We define an insult  $\Delta x$ , which is the unwanted PSF shift in wavenumber units, and define the reaction in the final spectrum to be  $\Delta \nu$ . We define the sensitivity to this error mode to be a Translation Reaction Coefficient (TRC),  $TRC \equiv \Delta x / \Delta \nu$ . For a conventional dispersive spectrograph,  $TRC = 1$ .

#### 4.2 Single Delay EDI Case

For a single delay EDI, the net TRC can be zero for an isolated narrow feature such as a ThAr line. This is because the phase of the moire fringe does change when the PSF shifts, because both the input spectrum and the underlying interferometer comb shift the same amount along the detector on the native spectrograph. This causes the moire phase to be constant.

However, this only holds true for isolated features. When there are a pair of features that are at least partially blended in the same native spectrograph resolution element, they create a moire pattern which can have a slope vs wavenumber. Then under a PSF shift, they can manifest a perceived shift in moire phase, which is an error, and causes the wavelet phase to shift in phase by the same amount. This corresponds to the red line in Fig. 10(b) that passes through the center of the EDI peak will have nonzero value on the edges of the peak.

An equivalent way of saying it is that the Fourier transform of a pair of blended ThAr lines can have energy unevenly distributed around the peak. Then when this is multiplied by the red line and the net reaction product

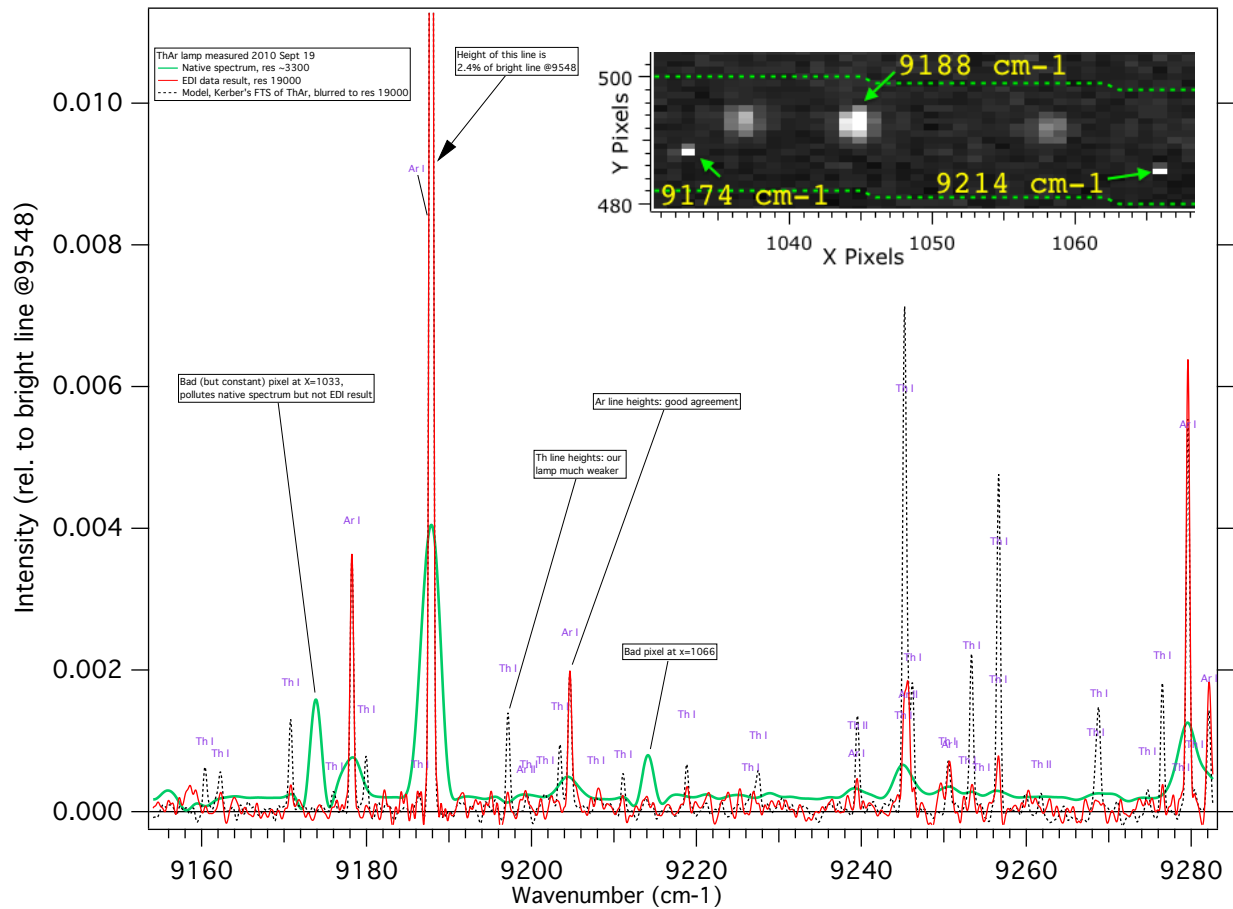


Figure 6. Measurement (red curve) of our ThAr lamp to a 6x boosted resolution of 19000, compared to NIST measurement<sup>19</sup> of a different ThAr lamp blurred to same resolution (black dashes), D-order. Purple text is their assignment of species. Native spectrograph (green curve) has resolution  $\sim 3300$ . Note disagreement in heights of Th lines, whereas Ar lines agree well, due to individuality of each ThAr lamp. Note extremely high dynamic range of measurement—  $\sim 0.1\%$  lines are easily observed (heights are fraction of  $9548 \text{ cm}^{-1}$  line). The EDI curve is robust to fixed pattern noise such as false peak in the native spectrum at  $9174$  and  $9214 \text{ cm}^{-1}$  due to bad pixels at  $X=1033$  and  $1066$  (inset shows detector there). Bad pixels are constant and thus do not affect whirls which look at changes between exposures.

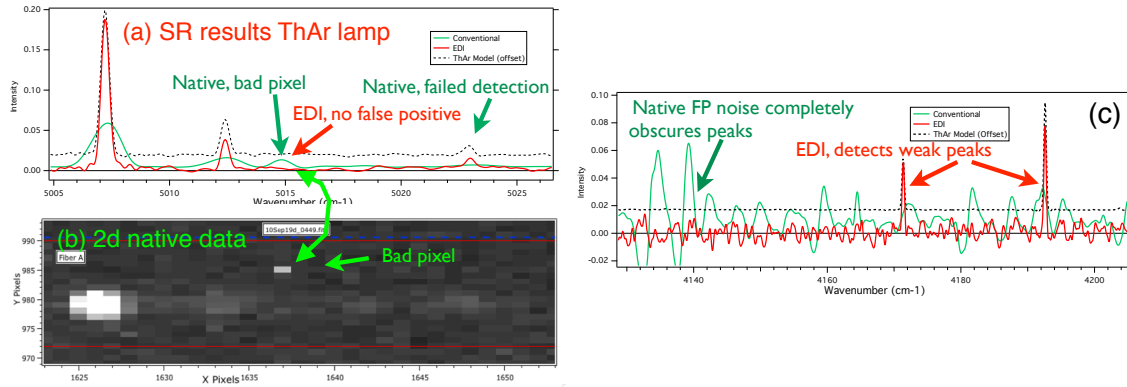


Figure 7. EDI is robust to fixed pattern (FP) errors that afflict the native spectrum, such as the false peak at  $5015\text{ cm}^{-1}$  (a) caused by a bad pixel (1637,985) shown in raw 2d data (b) of A-order. The EDI result (red curve) does not respond to this bad pixel because it does not vary sinusoidal with phase in the 10 exposures. (c) Another example is at extreme red end of the A-order ( $<4200\text{ cm}^{-1}$ ). The EDI is able to detect two very weak ThAr lines at  $4172$  and  $4193\text{ cm}^{-1}$ , whereas the native spectrum is not. Intensity axis is fraction of the  $4849\text{ cm}^{-1}$  line.

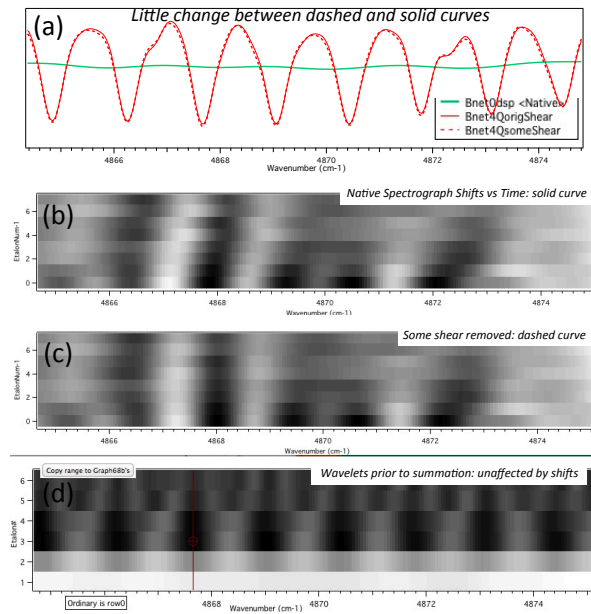


Figure 8. Demonstration in TEDI data of extreme robustness against irregular PSF shifts to the native spectrograph, due to use of multiple delays. (a) The 6-fold boosted spectral resolution (16,200 from 2,700) is achieved for the reconstructed spectrum (dashed and solid red curves) despite significant irregular wavenumber shift versus etalon number (Y), hence time, and vs wavenumber ( $\nu$ ) of the data. (b)(c) Native spectra vs etalon, (c) has bulk shear removed compared to (b). (b) Yielded solid red curve in (a), (c) yielded dashed red curve— little difference. Wavelets (d) summed to produce outputs (a). Green curve is native spectrum. Data of star HD219134, 2010 Sep 19, A-order.

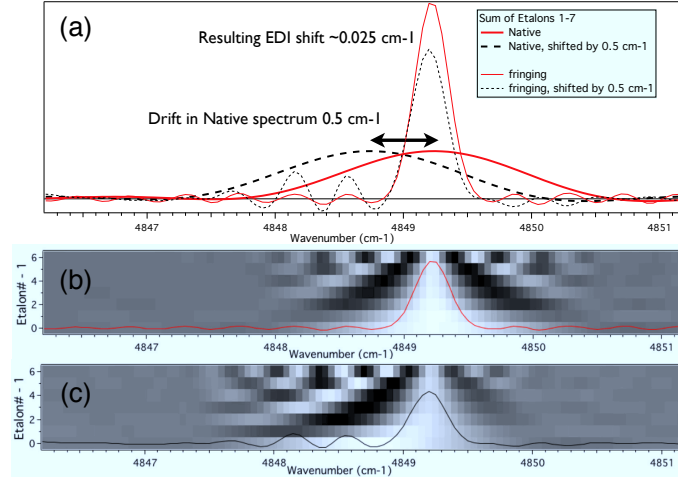


Figure 9. Simulated EDI reaction to a native spectrograph PSF translation using ThAr data and TEDI data processing. Moire input data becomes wavelets— a stack of 7 is shown in (b), which sum to produce a narrow peak in [a] (thin red curve) at  $\sim 16,000$  resolution (6x boost). (Unequalized gap between E6 and E7 delays produces slight ringing.) The effect of a PSF shift is simulated by translating every moire input by  $\Delta x = 0.5 \text{ cm}^{-1}$  to the left (c). Note shift in the envelope of the wavelet stack yet internal peaks are stationary. The summed peak (thin black) moves only  $\Delta \nu = 0.025 \text{ cm}^{-1}$  relative to the unshifted version (red peak), hence the Translational Reaction Coefficient,  $\Delta \nu / \Delta x = TRC = 0.05$ , a 20x reduction.

evaluated, the positive side (on the high delay side of the peak) and the negative side (on the low delay side of the peak) do not cancel in area. This causes a slight nonzero value for TRC.

However this TRC value is much smaller than unity, which is the TRC value for the native spectrograph. So even in the non-optimal case of blended lines, the single-delay EDI has a smaller reaction to PSF shift than a native spectrograph.

### 4.3 Case of Multiple Delays And Original Lineshapes

When multiple overlapping delays are used, as shown in Fig. 10(c) and Fig. 11, the positive reaction side of one peak can partially or totally cancel with the negative reaction side of a neighboring overlapped peak. When the original peak shapes are used, we find that the net reaction to a group of delays is not zero, but still small, having about  $TRC = 0.05$ . This was found both in the simulation Fig. 9 in wavenumber space, and the calculation Fig. 11(a) in frequency space.

Figure 11(a) shows the estimated net reaction for the set of peaks used by TEDI with their original shapes. Each peak was multiplied by a line going through its center delay, then these were summed over all peaks to produce the net reaction curve (thick black curve), which is consistent with the gray dashed line having slope  $TRC = 0.05$ . Note the sine-like shapes contributed by the isolated higher delays of E7 and E8 at 3 and 4.5 cm.

## 5. NEW CROSSFADING METHOD FOR FURTHER PSF DRIFT CANCELLATION

### 5.1 Case of Multiple Delays But Reshaped Lineshapes

We realized recently that we can reshape the peaks into triangle or sinc function shapes to enhance the cancellation between overlapping neighboring peaks and make the net reaction curve zero, for a region of frequency. We call this weighting choice “crossfading”. Figure 12(b)(c) shows that a triangle shape, when multiplied by a line, becomes a sine-like shape consisting of a pair of positive and negative parabolas. This shape, when shifted by a certain distance in delay or frequency space, flips its polarity. Hence if two triangle shapes are overlapping by this special distance, there is a region of frequency where there is perfect cancellation and  $TRC = 0$ . A sinc function and other shapes also satisfy this behavior, as described in more detail in Sect. 6.

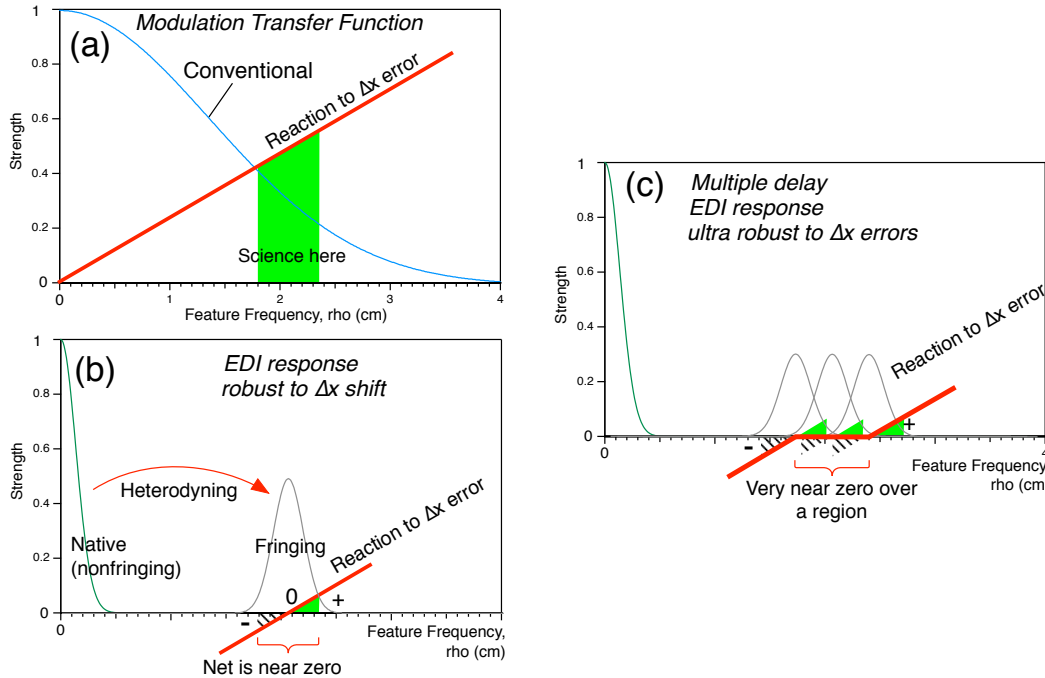


Figure 10. (a) The reaction of a conventional spectrograph to an unwanted displacement  $\Delta x$  along the dispersion direction at the detector, in Fourier space vs frequency  $\rho$ , is to multiply the  $psf(\rho)$  or  $MTF(\rho)$  by  $\rho$  (red line). Science frequencies typically are high (green band), producing a large reaction. (b) In contrast, for the EDI both the sensitivity peak and red line are shifted to high frequency by the interferometer delay, and the reaction flips polarity as  $\rho$  crosses the center of the peak. This can reduce the integrated reaction by an order of magnitude. (c) With a multiple delay EDI the net reaction is further reduced when the positive and negative portions of the peaks overlap.

The reshaping between the original and crossfading lineshape (as in Fig. 12(a)) is easily done by multiplying the data in Fourier space by a custom curve which is the ratio of the two shapes, similar to the equalization procedure. Hence it is essentially a numerical filtering.

Figure 11(b) shows the result for the net reaction curve for crossfading TEDI peaks that are re-shaped into a sinc function shape. Note how the net reaction curve (solid black) is zero between 0 and 1.8 cm where peaks are space sufficiently close to be overlapped. The two higher peaks E7 and E8 at 3 and 4.5 cm are too isolated to join with the crossfading scheme, but in principle additional delays could be purchased to allow overlap, such as delays at 2.3, 3.6 and 4 cm (our apparatus currently holds only eight glass etalons in the rotary “filter” holder).

### 5.2 Demonstration of Crossfading With a Simulated Spectrum

Figure 13 is a simulation with a simple source spectrum (a) consisting of a group of evenly spaced lines, to produce Fourier energy concentrated at a specific delay of 1.4 cm, so that only two delays at 1.2 and 1.6 cm are needed. The key point is that the moire patterns (b)(c) for a blended pair of features will manifest *opposite* slope, depending on whether the interferometer delay is higher or lower than the reciprocal spacing between the lines. Hence for two delays that bracket the source spectrum frequency, then under the same PSF wavenumber shift, the perceived moire phase shift (d) will be in *opposite* directions for the two patterns, and can cancel.

After lineshape reshaping, the final output spectrum (e) in the simulation is almost perfectly insensitive to a deliberate shift of the input moire data. The actual shift  $\Delta\nu = 0.0022 \text{ cm}^{-1}$  being 350 times smaller than the applied insult shift  $\Delta x$  of  $0.75 \text{ cm}^{-1}$  (TRC = 0.00293). This is remarkably small. A sinc function final lineshape was used here. A triangle final lineshape also produces a similarly small net shift but produces slightly more ringing.

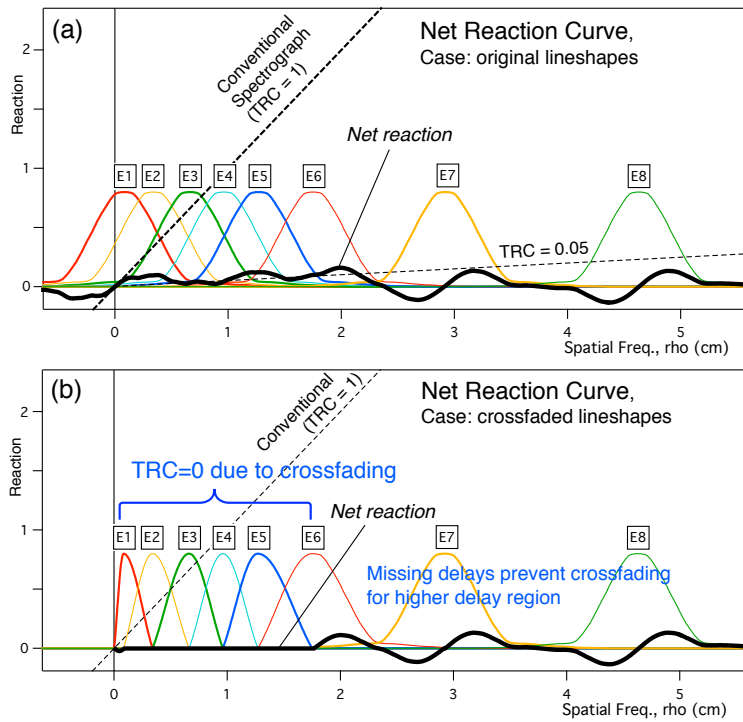


Figure 11. Net reaction (bold black curves) to a PSF  $\Delta x$  shift for set of TEDI peaks, for (a) original lineshape, and (b) peaks reshaped into a sinc function crossfading lineshape (triangle shape also works). Reaction is peak  $n$  shape (colored) multiplied by line  $(\rho - \tau_n)$  passing through peak center, then summed over  $n$ . (a) For original peak shapes, net reaction is consistent with same slope (gray dashes) of TRC=0.05 (translational reaction coefficient,  $\Delta\nu/\Delta x$ ) seen in Fig. 9. (b) Reshaped peaks cancel each others reaction so TRC=0. Remarkably, PSF can now drift in wavenumber without shifting the output spectrum– not possible in conventional spectroscopy where TRC=1 (black dashes). Missing delays at 2.3 and 3.8 cm prevent crossfading above 2 cm, (but TRC still less than 0.05). The TRC=0 region 0 to 1.8 cm allows 6x boost (16,000 resolution) in the A-order at  $4700\text{ cm}^{-1}$ . Crossfaded lineshapes are asymmetrical to achieve foot to center positioning for irregular delays  $\tau_n$ . Crossfading could potentially also include the native peak shape, but that is not done here.

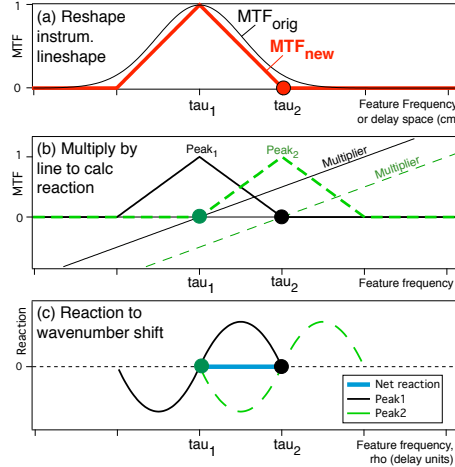


Figure 12. Achieving perfect PSF drift robustness between two delays  $\tau_1$  and  $\tau_2$  by crossfading using a triangular lineshape. This achieves zero net translational reaction (TRC=0) for frequency  $\rho$  between the peaks (frequency and delay have same units). (a) The  $psf(\rho)$  or MTF for each peak is reshaped to a crossfading shape, here a triangle, by multiplication of data in  $\rho$ -space by  $(MTF_{new}(\rho)/MTF_{orig}(\rho))$ . (b) For dual-peak crossfading, foot of  $peak_1$  (black dot) must be 0% at  $\tau_2$ , which is maximum of neighboring  $peak_2$  (green dash triangle), and vice versa for  $peak_2$  foot (green dot) at  $\tau_1$ . Reaction to a wavenumber shift  $\Delta x$  is estimated by multiplying MTF by line through center of each peak. (c) For triangular peak this creates a sine-like odd-symmetry shape consisting of two opposite parabolas. (For sinc function, it makes an exact sinusoid.) When overlaid with the identical but shifted sine-like shape of the neighboring peak (dashed), the net reaction (bold blue segment) is zero between  $\tau_1$  and  $\tau_2$ . (The  $\Delta x$  presumed same for both peaks.) Scheme is extended to all pairs of peaks  $\tau_n$  to  $\tau_{n+1}$  to cover all delay space with TRC=0. For unevenly spaced peaks, reshaped peaks are asymmetrical.

This crossfading work is preliminary and we have not yet applied it to bulk TEDI data. We are exploring what is the optimal shape and what effects limit the performance. For example, the actual PSF shape may vary slightly across the band.

Given the realization that TRC could in principle be made zero over a range of frequencies, this implies that EDI apparatus that measure radial velocities for the Doppler planet search should be modified to use two delays that are overlapping in delay space and ideally measuring the same spectrum simultaneously (so that the same insult applies to both peaks). Figure 14 shows a notional schematic of how to measure two or more delays simultaneously using a stepped mirror.

## 6. DETAILS OF CROSSFADING METHOD TO CANCEL PSF DRIFT

### 6.1 General Lineshape for Two Crossfading Peaks

To engineer perfect cancellation of the net reaction of overlapped peaks, the shape and width of the peaks are modified into a so-called “crossfading” shape. The original psf is reshaped to a new psf by multiplying the data in Fourier space with a multiplier  $[psf_{new}(\rho)/psf_{orig}(\rho)]$ , as in Fig. 12(a) from a typical peak with gradual wings into a triangle crossfading shape having a well defined width. For the dual peak crossfade discussed here (mixing more peaks is possible), the most important consideration is that the edge of the  $peak_1$  (called a “foot”) goes to zero magnitude at the center position  $\tau_2$  of the neighboring  $peak_2$ , and stays zero beyond that.

From the isolated peaks E7 and E8 of Fig. 11(a) one can see that each peak produces a odd symmetry sine-like contribution to the reaction curve, with the right side being positive and the left negative. The new idea is to reshape the peaks to overlap so that the positive contribution of one peak perfectly cancels the negative contribution of the neighboring peak. This is illustrated in Fig. 12(b)(c) for the simple case of a triangle lineshape. Between the two peaks, i.e. between  $\tau_1$  and  $\tau_2$ , a crossfading is said to occur.

There are a family of curves that satisfy this condition of producing TRC=0 in this crossfade region between the peaks. Let us derive the equation that describes them. The net reaction to a horizontal PSF drift is the

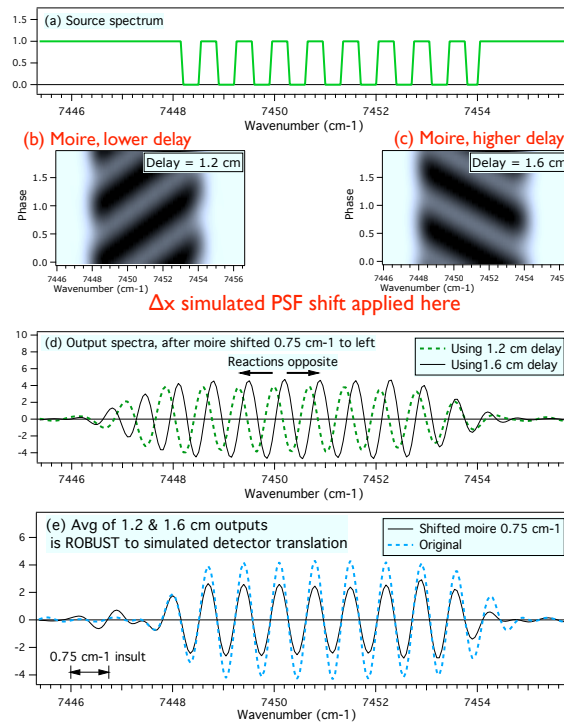


Figure 13. Demonstration of the crossfading weighting technique on a simulated spectrum (a) consisting of several rectangular lines spaced  $0.7 \text{ cm}^{-1}$ , so that Fourier energy (at  $\sim 1.4 \text{ cm}$ ) is between overlapping delay peaks at 1.2 and 1.6 cm. Moires for the smaller (b) and larger (c) delays have *opposite* polarity slopes, and thus react oppositely in phase to a simulated PSF drift of  $\Delta x = 0.75 \text{ cm}^{-1}$  to left. The net reaction can be cancelled by strategic shaping of lineshape prior to combining (sinc function shape was used, triangle produces slightly more ringing). (d) Peaks in output spectra for 1.2 cm (green dash) and 1.6 cm (black) delays react oppositely, (and differently than the envelope which shifts to left). Average of the 1.2 and 1.6 curves forms the final outputs (e), for original (blue dash) and artificially shifted (black) moire positions. Peaks appear in their original positions, robust to the moire shift. Change in peak position between blue dash and black curves is only  $0.0022 \text{ cm}^{-1}$ , 350 times smaller than the simulated PSF drift of  $0.75 \text{ cm}^{-1}$ . That is, TRC  $\sim 0.003$ .

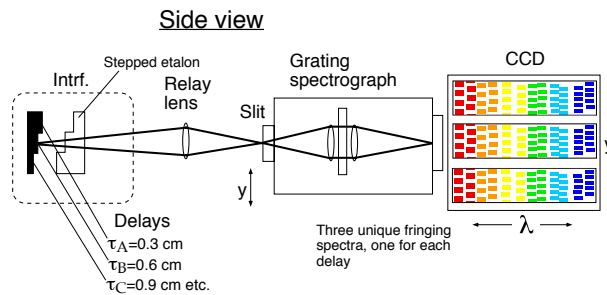


Figure 14. Notional diagram of stepped mirror scheme<sup>3</sup> for measuring multiple delays simultaneously with the same disperser, so that short term PSF spectrograph drifts can be shared among at least two delays, to cancel drift using crossfaded data mixing. Staircase stepped shape of mirror and glass etalon of interferometer (dashed square) images different delays to different detector pixels, but passes through same disperser. This is undesirable if drifts are pixel row dependent. However, the stepped mirror could be combined with TEDI's swapped delay scheme that uses same pixel rows, to discover both long and short term drifts on the same pixels for at least two delays.

product of the line  $(\rho - \tau_n)$  through the center of the peak, times each peak. For  $n$  peaks this is

$$Reaction(\rho) \propto \sum (\rho - \tau_n) psf(\rho - \tau_n). \quad (1)$$

To produce perfect cancellation between two overlapping peaks of same shape  $psf(\rho - \tau_1) \equiv f(r)$ , and  $psf(\rho - \tau_2) = f(r - 1)$ , and using a dimensionless frequency  $r = (\rho - \tau_1)/|\tau_2 - \tau_1|$  centered at the left peak, #1, we must satisfy

$$rf(r) + (r - 1)f(r - 1) = 0 \quad (2)$$

which is equivalent to satisfying, when  $F(r) = rf(r)$ ,

$$F(r) + F(r - 1) = 0. \quad (3)$$

## 6.2 Case of Triangle Lineshape

The simplest case is a triangle lineshape, separated by distance 1 and height 1, which thus has linear crossfading of unity slope between the peaks. Then the right side of the left peak is  $f(r) = 1 - r$ , so the first term of Eq. 2 is  $r(1 - r)$ , and the left side of the right peak is  $r$  so the 2nd term is  $(r - 1)r$ . Hence Eq. 2 is satisfied since  $r(1 - r) + (r - 1)r = 0$ , and in the region between the two peaks  $TRC=0$ .

We apply this crossfade reshaping to every pair of overlapping peaks to fill a contiguously overlapped  $\rho$  region entirely with  $TRC=0$ . For the case of irregular  $\tau_n$ , the peaks will be asymmetrical, treated as half-peaks, in order to always place the foot on the center of the neighboring peak and vice versa. That is, the left half of peak at  $\tau_{n+1}$  is the reflection of right half of peak at  $\tau_n$ , and these can be a different shape than neighboring pairs of half-peaks. So one should view a manifold of peaks as instead a manifold of crossfading pairs of half-peaks.

## 6.3 Other Crossfading Lineshapes

Besides a triangle shape, a sinc function,  $f(r) = \sin(\pi r)/r$ , for just the region between its first zeros, also satisfies Eq. 2. This produces  $F(r) = \sin(\pi r)$ , which has the required property that shifting by 1 flips its polarity. This has the advantage of a rounded peak that avoids some possible ringing produced by the sharp tip of a triangle. Interestingly, the sinc function (but with its many satellite peaks) is the Fourier transform of a rectangle and hence is naturally the psf of a slit opened much wider than its spectrograph focal blur. We are studying the utility of other crossfading shapes that satisfy Eq. 2.

## 6.4 Correlated PSF Drifts Needed

The above crossfading method presumes that the *same*  $\Delta x$  PSF drift applies to the two overlapped delay peaks. Otherwise the cancellation will be incomplete. This is naturally satisfied by long term drifts in a TEDI style apparatus which measures delays sequentially on the same pixels using different glass etalons that are rotated into the interferometer beam, where “long” means longer than the time to measure each delay (typically several minutes).

We propose that shorter term drifts would be more correlated between peaks by using a stepped mirror (Fig. 14) which can be designed to manifest several delays simultaneously from the same source, although on different detector pixel rows. Then comparison of original (having shift) to crossfaded data (having no shift) yields information on the PSF shift  $\Delta x$ , which thus could be at short times scales as well as long. However, this would be susceptible to any row dependence to the  $\Delta x$  drifts (such as thermally induced on the detector, and thus likely to be long time scale).

By combining in the same apparatus a stepped mirror with a sequentially changed etalon similar to TEDI, information on short timescale variations from the stepped mirrors but on different pixel rows could be joined with that sequentially measured on the same rows. We speculate that this could produce a near zero TRC apparatus for Doppler velocimetry or high resolution spectroscopy that was robust both on long and short timescales. The details of how to combine the data to best tease out the desired information are still under investigation.

## 7. MOTIVATION: PSF DRIFT

### 7.1 Motivation: Dispersive Spectrographs Suffer From PSF Drifts

One of the most significant technical challenges in the field of high resolution spectroscopy and Doppler radial velocimetry in the quest to achieve sub meter per second accuracy over long term time scales is the prevention of, or subsequent compensation for, changes in the calibration of the spectrograph. This is driven by the desire to detect and characterize small exoplanets,<sup>20</sup> as well as the capability to detect cosmological changes over many years.<sup>21</sup> Instrumental caused drifts and irregularities include changes in the focal spot or centroid of the spectrograph point spread function (PSF) relative to the detector, or irregularities in the perceived placement of detector pixels through manufacturing errors or through nonideal spectrograph optics.

This involves many times scales, from rapid atmospheric fluctuations, to multi-month drifts, and involves many distance scales along the dispersion axis, from a few pixels between a stellar spectral feature to the nearest reference spectrum feature, to the entire bandwidth when the detector shifts monolithically due to thermal or changes in gravity vector. Sources of wavenumber drift of the calibration include atmospheric fluctuations, thermal changes, gravity vector changes, pupil changes which illuminate different set of grating grooves, changes in optical fiber transmission modes in fiber scramblers or conduction from telescope to spectrograph. It also includes static irregularities such as nonuniform placement of detector pixels when such irregularities interact with large changes in wavenumber of the stellar or reference spectra, such as due to 6 months of the motion of the Earth in its orbit, or thermomechanical shifts. In that case, the static irregularities become time dependent, and thus manifest errors even though offsets have been properly subtracted from data.

### 7.2 Traditional Instrumental Strategies

Traditional preventive remedies include placing the spectrograph in thermally controlled environments including vacuum tanks, and sending light through fiberoptic scramblers.<sup>22</sup> Such remedies are usually expensive, heavy, and the use of fibers can create a flux penalty. The increased weight and bulk of a thermally stable vacuum enclosure prevents use in weight and space critical platforms such as aircraft and spacecraft. It is also one of the main reasons why the many moderate size telescopes operated by many small universities and institutions are not participating more in the Doppler planet search, because the difficulty in constructing and operating a spectrograph of sufficient resolution and long term stability of calibration can be prohibitively costly for that size institution.

An early line of defense against an unknown drift is to measure a reference spectra as simultaneously (spatially and temporally) as possible to the stellar spectra. However, many commonly used reference spectra, such as a ThAr spectral lamp or iodine transmission cell do not have spectral features everywhere, so there is some distance, typically a few wavenumbers or tens of wavenumbers, between a stellar feature and a significantly strong reference feature. Over that distance the irregularity of the disperser's calibration can change. Laser spectral combs can provide a uniform grid of spectral features but tend to be costly.

## 8. CONCLUDING DISCUSSION

### 8.1 Implications for Precision Radial Velocimetry

In light of the great advantage of having at least two overlapping delays to cancel the effect of PSF drift, we encourage users of single delay EDI for velocimetry to consider modifying their apparatus to measure two or more delays quasi-simultaneously, such as in Fig. 14. Or if their existing single delay overlaps their native peak, they can apply crossfading to mix native and single delay signals, for frequencies up to but not beyond the delay. The decrease in TRC should directly reduce a horizontal (wavelength) noise, translating into reduced Doppler velocity noise if PSF translation is the dominant type of insult, and if not dominated by photon or read noise. (Example noise sources not addressed by the TRC could be telluric contributions that are time varying and blended into the spectrum, or spatial drifts in the reference ThAr beam relative to the stellar beam, causing slight differential phase shifts in the interferometer.)

## 8.2 Combined Benefit of Crossfading With Environmental Control

The instrument error that results is a product of two factors: the magnitude of applied insult (e.g.  $\Delta x$ ), times the sensitivity (e.g. TRC) of the instrumental technique to such insult. Optimally, both of these factors should be reduced for a precision radial velocimeter or high resolution spectrograph. This paper focuses on the latter (sensitivity) factor. Previously, it was not possible to reduce the TRC of a conventional dispersive spectrograph—it is fixed at unity, so naturally effort by the community was to reduce the former factor, such as by environmental stabilization, fiber scrambling etc.

Now we have shown that both factors can be reduced. Using an EDI with multiple delays we can reduce TRC by at least a factor of 20 by using our standard processing (which uses original lineshapes). Remarkably, an order of magnitude further reduction of TRC is possible with strategic reshaping of the lineshape in the data using the so-called crossfading method. Because these two benefits multiply, even a spectrograph which is environmentally stabilized can benefit from the inclusion of an interferometer (which can be outside the spectrograph environmental enclosure where it is simple to access, or in its own smaller enclosure).

## 8.3 EDI as Local Spectral Comb Calibrant

The EDI can be thought of as providing a local spectral comb calibration apart from the absolute calibration reference spectrum (which is expected to be used also). Distortions that shift the spectrograph PSF also shift the perceived spectral comb, which causes the created moire patterns to be intrinsically less sensitive to these PSF shifts, by an order of magnitude, since the heterodyning signals work off the positional difference between the input spectrum and the comb. Yet these moire patterns still have a nonzero sensitivity to these PSF shifts, even if smaller by  $\sim 20x$  (as seen in Fig. 9). Now with the new crossfading technique, the moire patterns sensitivity can be made, theoretically, completely insensitive to the PSF shifts.

Since an absolute spectral reference is expected to also be used in an EDI, as with a conventional spectrograph, one might ask, why is there a PSF shift issue? The reason is that most convenient and affordable spectral references have an uneven density distribution of features, so there are some wavenumber regions which are not sufficiently covered by calibrant features. And Fig. 3 shows that the PSF distortion can be irregular on a few wavenumber scale. Hence a perfect insensitivity to PSF shift, which crossfading may provide, would be a very desirable feature to address these regions insufficiently covered by the absolute spectral reference.

## ACKNOWLEDGMENTS

This material is based upon work supported by the National Science Foundation under Grant No. AST-0505366, AST-096064, NASA Grant NNX09AB38G, and by Lawrence Livermore National Laboratory under Contract DE-AC52-07NA27344.

## REFERENCES

- [1] Erskine, D. J., “An externally dispersed interferometer prototype for sensitive radial velocimetry: theory and demonstration on sunlight,” *PASP* **115**, 255–269 (2003).
- [2] Erskine, D. J. and Ge, J., “Novel Interferometer Spectrometer for Sensitive Stellar Radial Velocimetry,” in [*Imaging the Universe in Three Dimensions: Astrphys. Advncd. Multi-Wavel. Imaging Devices*], van Breugel, W. and Bland-Hawthorn, J., eds., *ASP Conf. Series* **195**, 501–507 (2000).
- [3] Erskine, D. J., “Combined dispersive/interference spectroscopy for producing a vector spectrum,” *US Patent* **6,351,307** (Issued Feb. 26, 2002).
- [4] Ge, J., van Eyken, J., Mahadevan, S., DeWitt, C., Kane, S. R., Cohen, R., Vanden Heuvel, A., Fleming, S. W., Guo, P., Henry, G. W., Schneider, D. P., Ramsey, L. W., Wittenmyer, R. A., Endl, M., Cochran, W. D., Ford, E. B., Martín, E. L., Israelian, G., Valenti, J., and Montes, D., “The first extrasolar planet discovered with a new-generation high-throughput Doppler instrument,” *ApJ* **648**, 683–695 (2006).
- [5] Edelstein, J., Muterspaugh, M. W., Erskine, D. J., Feuerstein, W. M., Marckwordt, M., Wishnow, E., Lloyd, J. P., Herter, T., Muirhead, P., Gull, G. E., Henderson, C., and Parshley, S. C., “TEDI: the TripleSpec Exoplanet Discovery Instrument,” in [*Society of Photo-Optical Instrumentation Engineers (SPIE) Conference Series*], *Proc. SPIE* **6693** (2007).

- [6] Mahadevan, S., Ge, J., Fleming, S. W., Wan, X., DeWitt, C., van Eyken, J. C., and McDavitt, D., “An inexpensive field-widened monolithic michelson interferometer for precision radial velocity measurements,” *PASP* **120**, 1001–1015 (2008).
- [7] Muirhead, P. S., Edelstein, J., Erskine, D. J., Wright, J. T., Muterspaugh, M. W., Covey, K. R., Wishnow, E. H., Hamren, K., Andelson, P., Kimber, D., Mercer, T., Halverson, S. P., Vanderburg, A., Mondo, D., Czeszumaska, A., and Lloyd, J. P., “Precise stellar radial velocities of an M dwarf with a Michelson interferometer and a medium-resolution near-infrared spectrograph,” *PASP* **123**(904), 709–724 (2011).
- [8] van Eyken, J. C., Ge, J., and Mahadevan, S., “Theory of Dispersed Fixed-delay Interferometry for Radial Velocity Exoplanet Searches,” *ApJS* **189**, 156–180 (2010).
- [9] Jensen-Clem, R., Muirhead, P. S., Bottom, M., Wallace, J. K., Vasisht, G., and Johnson, J. A., “Attaining Doppler Precision of 10 cm/s with a Lock-In Amplified Spectrometer,” *Publications of the Astronomical Society of the Pacific* **127**(957), 1105–1112 (2015).
- [10] Erskine, D. J. and Edelstein, J., “High-resolution Broadband Spectral Interferometry,” in [*Future EUV/UV and Visible Space Astrophysics Missions and Instrumentation*, ed. J. C. Blades, O. H. Siegmund], *Proc. SPIE* **4854**, 158–169 (2003).
- [11] Erskine, D. J., Edelstein, J., Feuerstein, M., and Welsh, B., “High resolution broadband spectroscopy using an externally dispersed interferometer,” *ApJ* **592**, L103–L106 (2003).
- [12] Erskine, D. J. and Edelstein, J., “Interferometric resolution boosting for spectrographs,” in [*Ground-based Instrumentation for Astronomy*], Moorwood, A. and Iye, M., eds., *Proc. SPIE* **5492**, 190–199 (2004).
- [13] Erskine, D. J., Edelstein, J., Muirhead, P., Muterspaugh, M., Covey, K., Mondo, D., Vanderburg, A., Andelson, P., Kimber, D., Sirk, M., and Lloyd, J., “Ten-fold spectral resolution boosting using TEDI at the Mt. Palomar NIR Triplespec spectrograph,” in [*UV/Optical/IR Space Telescopes and Instruments: Innovative Technologies and Concepts V*], Tsakalakos, L., ed., *Proc. SPIE* **8146** (2011).
- [14] Edelstein, J., Erskine, D. J., Sirk, M., Vanderburg, A., and Wishnow, E. H., “Enhanced spectral resolution via externally dispersed interferometry,” in [*Ground-based and Airborne Instrumentation for Astronomy IV*], Ian McLean, S. Ramsay, H. T., ed., *Proc. SPIE* **8446** (2012).
- [15] Erskine, D. J., Edelstein, J., Sirk, M., Wishnow, E., Ishikawa, Y., McDonald, E., and Shourt, W. V., “High Resolution Broad-Band Spectroscopy in the NIR Using the TripleSpec Externally Dispersed Interferometer at the Hale Telescope,” in [*Ground-based and Airborne Instrumentation V*], *Proc. SPIE* **9147**, 914717 (2014).
- [16] Erskine, D. J., Edelstein, J., Wishnow, E. H., Sirk, M., Muirhead, P. S., Muterspaugh, M. W., Lloyd, J. P., Ishikawa, Y., McDonald, E. A., Shourt, W. V., and Vanderburg, A. M., “High-resolution broadband spectroscopy using externally dispersed interferometry at the Hale telescope: Part 1, data analysis and results,” *J. Astron. Tele. Instr. Sys.* **2**(2), 025004 (2016).
- [17] Erskine, D. J., Edelstein, J., Wishnow, E., Sirk, M., Muirhead, P. S., Muterspaugh, M. W., and Lloyd, J. P., “High Resolution Broad-Band Spectroscopy Using Externally Dispersed Interferometry at the Hale Telescope: Part 2, Photon Noise Theory,” *J. Astron. Tele. Instr. Sys.* (submitted Feb 2016).
- [18] Wilson, J. C., Henderson, C. P., Herter, T. L., Matthews, K., Skrutskie, M. F., Adams, J. D., Moon, D.-S., Smith, R., Gautier, N., Ressler, M., Soifer, B. T., Lin, S., Howard, J., LaMarr, J., Stolberg, T. M., and Zink, J., “Mass producing an efficient NIR spectrograph,” in [*Ground-based Instrumentation for Astronomy*], Moorwood, A. and Iye, M., eds., *Proc. SPIE* **5492**, 1295–1305 (2004).
- [19] Kerber, F., Nave, G., and Sansonetti, C. J., “The Spectrum of Th-Ar Hollow Cathode Lamps in the 691-5804 nm region: Establishing Wavelength Standards for the Calibration of Infrared Spectrographs,” *ApJS* **178**, 374–381 (2008).
- [20] Butler, R., Marcy, G., Williams, E., McCarthy, C., Dosanjh, P., and Vogt, S., “Attaining Doppler Precision of 3 m/s,” *PASP* **108**, 500 – 509 (1996).
- [21] Kim, A. G., Linder, E. V., Edelstein, J., and Erskine, D., “Giving Cosmic Redshift Drift a Whirl,” *Astropart. Phys.* **62**, 195 – 205 (2015).
- [22] Halverson, S., Roy, A., Mahadevan, S., Ramsey, L., Levi, E., Schwab, C., Hearty, F., and MacDonald, N., “An Efficient, Compact, and Versatile Fiber Double Scrambler for High Precision Radial Velocity Instruments,” *ApJ* **806**, 61 (2015).